ACS APPLIED MATERIALS & INTERFACES

Research Article

www.acsami.org

Low-Band-Gap Conjugated Polymers of Dithieno[2,3-*b*:7,6-*b*]carbazole and Diketopyrrolopyrrole: Effect of the Alkyl Side Chain on Photovoltaic Properties

Yunfeng Deng,[†,‡] Yagang Chen,[†,‡] Jian Liu,[†,‡] Lihui Liu,[†,‡] Hongkun Tian,[†] Zhiyuan Xie,[†] Yanhou Geng,*[,†] and Fosong Wang[†]

[†]State Key Laboratory of Polymer Physics and Chemistry, Changchun Institute of Applied Chemistry, Chinese Academy of Sciences, Changchun 130022, People's Republic of China

[‡]University of Chinese Academy of Sciences, Beijing 100049, People's Republic of China

Supporting Information

ABSTRACT: Four donor−acceptor (D−A) conjugated polymers of dithieno[2,3-*b*;7,6-*b*]carbazole (DTC) and diketopyrrolopyrrole, which have different alkyls on the nitrogen atom in the DTC unit and are named as **P-C8C8**, **P-C5C5**, **P-C12**, and **P-C10**, respectively, have been synthesized for studying the effect of the alkyl side chains on the optoelectronic properties of the polymers. All polymers are soluble in various organic solvents and exhibit identical optical band gaps (E_g^{opt}) of ∼1.3 eV and highest occupied molecular orbital energy levels of ∼−5.1 eV. Organic thin-film transistors and bulk heterojunction polymer solar cells (BHJ PSCs) with phenyl-C_{71}-butyric acid methyl ester ($PC_{71}BM$) as the electron-accepting material were fabricated via solution spin-casting. Compared to the polymers substituted by branched alkyl chains, the polymers with straight alkyl chains show higher hole mobility. Of these polymers, **P-C10** exhibits the highest field effect mobility up to 0.011 $cm^2/V{\cdot}s$. The alkyl chain on the DTC unit has a strong impact on the film morphology of polymer:$PC_{71}BM$ blends. Severe phase separation was found for polymers containing branched alkyl chains, and those with straight alkyl chains formed uniform films featuring fine phase separation. An open-circuit voltage (V_{oc}) of 0.72 V, a short-circuit current density (J_{sc}) of 13.4 mA/cm^2, a fill factor (FF) of 62%, and a power conversion efficiency (PCE) of 5.9% were demonstrated for BHJ PSCs based on the **P-C10**:$PC_{71}BM$ [1:3 (w/w)] blend film.

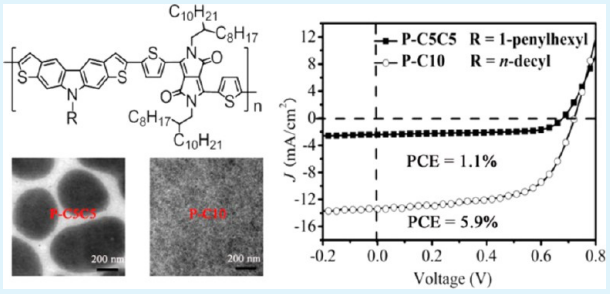

KEYWORDS: *conjugated polymers, polymer solar cells, low band gap, film morphology, alkyl chain effect, power conversion efficiency*

1. INTRODUCTION

Bulk heterojunction polymer solar cells (BHJ PSCs) have attracted much attention because they can be fabricated by low-cost roll-to-roll printing techniques.[1−3] Over the last several years, significant progress has been made in the area of BHJ PSCs, and the power conversion efficiency (PCE) of BHJ PSCs has reached 7−9% owing to the development of novel donor polymers and device architectures.[4−16] These achievements also open up new opportunities to improve the PCE of BHJ PSCs beyond 10%.

In order to harvest solar light efficiently, it is very necessary to reduce the optical band gap (E_g^{opt}) of the active materials. Therefore, the design and synthesis of low-band-gap conjugated polymers as electron-donating materials for BHJ PSCs have attracted remarkable attention during the past decade. Several strategies have been proposed for lowering the band gap of conjugated polymers.[17−19] Of those, copolymerizing electron-rich and electron-deficient aromatic moieties to form donor−acceptor (D−A) conjugated polymers is the most common approach for ease of band-gap and energy level manipulation. In this regard, a number of donor and acceptor units have been developed for the construction of D−A low-band-gap conjugated polymers.[20−37] Among the donor units, polyaromatics are very promising because the planarization of polyaromatic frameworks can facilitate π-electron delocalization and increase the effective conjugation length, providing an effective way to reduce the band gap. Meanwhile, polyaromatics also possess low reorganization energy, which could enhance the charge mobility of the resulting D−A conjugated polymers.[22,26−33]

Carbazole is a D building block that has been widely used to construct D−A conjugated polymers. Its derivatives possess deep highest occupied molecular orbital (HOMO) energy levels and good hole-transporting properties, which are important for realizing high open-circuit voltages (V_{oc}) and short-circuit currents (J_{sc}), respectively. One particular D−A conjugated polymer based on carbazole, **PCDTBT**, has revealed a PCE beyond 6%.[21,37,38] Several polyaromatic D

Received: April 5, 2013
Accepted: May 29, 2013
Published: May 29, 2013

   dx.doi.org/10.1021/am401175v | ACS Appl. Mater. Interfaces 2013, 5, 5741−5747

Scheme 1. Synthetic Route of the Monomers and Polymers[a]

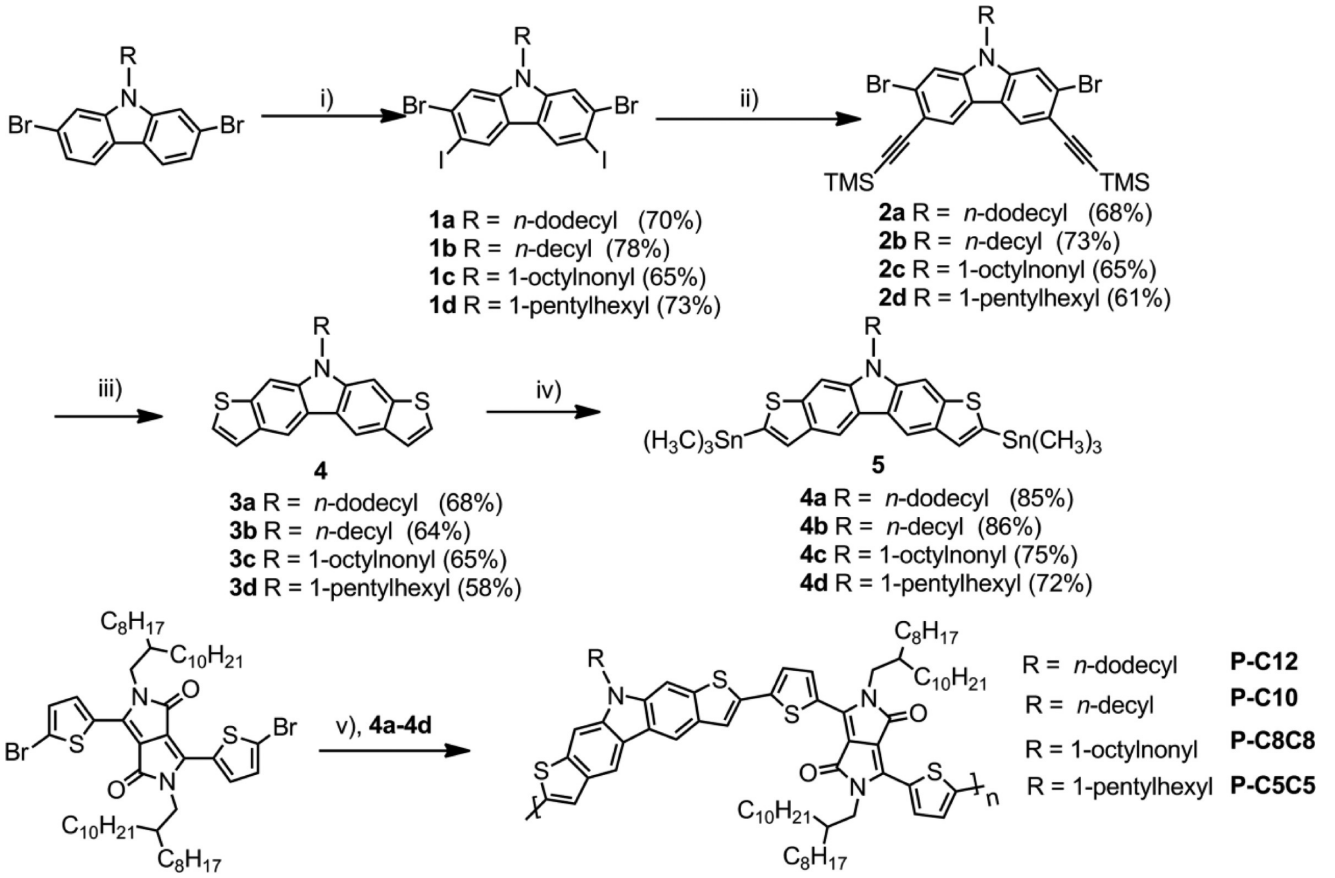

[a]Reagents and conditions: (i) KI, KIO_3, AcOH, 80 °C; (ii) (trimethylsilyl)acetylene, $Pd(PPh_3)_2Cl_2$, CuI, Et_3N, THF, room temperature; (iii) $Na_2S{\cdot}9H_2O$, NMP,190 °C; (iv) *n*-BuLi, Me_3SnCl, THF, −78 °C to room temperature; (v) $Pd_2(dba)_3$, P(*o*-tol)$_3$, toluene, 120 °C.

building blocks based on carbazole have also been developed to construct D−A conjugated polymers for BHJ PSCs. For instance, Hsu et al. reported a carbazole-based polyaromatic with seven fused rings, and its copolymers with different A units exhibited PCE up to 4.6%.[29] Afterward, they found that the PCE could be further enhanced to 5.2% upon optimization of the structure of the D unit.[31] Recently, we reported a new heteroarene based on carbazole, i.e., *N*-dodecyldithieno[2,3-*b*:7,6-*b*]carbazole (DTC), in which two outer thiophene rings are fused on the carbazole core, forming a planar π-conjugated system.[39] Its D−A conjugated polymer with diketopyrrolopyrrole (DPP), i.e., **P-C12**, exhibited an optical band gap of 1.35 eV and a field-effect hole mobility of 6.7×10^{-3} cm^2/V·s.[40] This implies that the polymers based on DTC and DPP are promising low-band-gap donor materials for BHJ PSCs. Moreover, it has been reported that the alkyl side chains significantly influence the performance of BHJ PSCs because they have a noticeable impact on the packing structures of the polymer backbone or the miscibility between polymer and fullerene derivatives.[41−45] Thus, in the current paper, we synthesized a series of D−A conjugated polymers of DTC and DPP units, in which different alkyl chains on the nitrogen atom in the DTC unit were employed. The photophysical, charge-carrier-transporting, and photovoltaic properties of the resulting polymers were studied in detail.

2. EXPERIMENTAL SECTION

Materials and Synthesis. Tetrahydrofuran (THF) and toluene were distilled after drying with sodium in the presence of benzophenone. Et_3N, acetonitrile, and CH_2Cl_2 were dried with CaH_2 and distilled before use. 3,6-Bis(5-bromothiophen-2-yl)-*N*,*N*′-(2-octyldodecyl)-1,4-diketopyrrol[3,4-*c*]pyrrole was synthesized according to a literature report.[41] Other reagents were used as received from commercial resources without further purification. The synthesis and characterization of the monomers and polymers are outlined in the Supporting Information (SI).

Fabrication and Measurements of Organic Thin-Film Transistors (OTFTs). OTFTs were fabricated by solution spin-casting on heavily doped n-type silicon wafers with 300 nm thermally grown SiO_2 (C_i = 10 nF/cm^2) following the procedure reported previously.[40] The substrate was modified with octylsilyltrichloride (OTS-C8) before deposition of the polymer layer. Polymer solutions in *o*-dichlorobenzene (*o*-DCB) with a concentration of 6 mg/mL were used for spin-casting. Thermal annealing of the polymer films was conducted in a glovebox. The channel width (W) and length (L) of the OTFTs were 3000 and 100 μm, respectively. The device performance was measured with two Keithley 236 source/measure units in an ambient atmosphere.

Fabrication and Measurements of BHJ PSCs. BHJ PSCs with a device structure of ITO/PEDOT:PSS (40 nm)/polymer:$PC_{71}BM$ (90 nm)/LiF (1 nm)/Al (100 nm) were fabricated and characterized following the procedure reported previously.[46] The blend films of polymer:$PC_{71}BM$ were prepared by spin-casting from *o*-DCB solutions in a glovebox. The devices were encapsulated in the glovebox before measurement in air, and the device area was 0.124 cm^2.

3. RESULTS AND DISCUSSION

Synthesis of the Polymers and Their Thermal Stability. Scheme 1 shows the synthetic route of the monomers and polymers. The polymers were synthesized via a Stille coupling reaction with $Pd_2(dba)_3/P(o\text{-tol})_3$ as the catalyst in yields of 80−87%. All polymers were purified by multiprecipitation and Soxhlet extraction with acetone, hexane, and chloroform in succession. They are soluble in common organic solvents such as THF, chloroform, chlorobenzene (CB), and *o*-DCB. The number-average molecular weights (M_ns) and polydispersity indices (PDIs) are in the range of 18−46 kDa and 2.31−2.92, respectively, as measured by gel permeation chromatography (GPC) with polystyrene as the standard (Table 1).

Table 1. M_ns, Weight-Average Molecular Weights (M_ws), PDIs, and Thermal Decomposition Temperatures (T_ds) of the Polymers

polymer	M_n (kDa)[a]	M_w (kDa)[a]	PDI[a]	T_d (°C)[b]
P-C8C8	46.6	107.6	2.31	367
P-C5C5	27.9	73.4	2.63	378
P-C12	18.8	46.3	2.46	402
P-C10	16.8	49.1	2.92	400

[a]Molecular weights and PDIs were measured by GPC at 40 °C with THF as the eluent and polystyrene as the standard. [b]Reported as the temperature with 5% weight loss.

The thermal stability of the polymers was evaluated by thermogravimetric analysis (TGA) in nitrogen with a heating rate of 10 °C/min. As shown in Figure 1 and Table 1, all

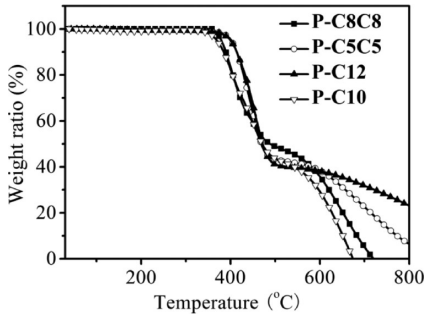

Figure 1. TGA plots of the polymers at a heating rate of 10 °C/min in a nitrogen atmosphere.

polymers are thermally stable with decomposition temperatures (T_ds) above 360 °C. Differential scanning calorimetry (DSC) analysis was performed in nitrogen with a heating/cooling rate of ±10 °C/min. No thermal transitions were observed for all four polymers at temperatures below 320 °C (Figure S1 in the Supporting Information).

Photophysical and Electrochemical Properties. Solution and film absorption spectra of the polymers **P-C8C8**, **P-C5C5**, **P-C12**, and **P-C10** were measured to examine the effect of alkyl substituents on their photophysical properties. All polymers show absorption spectra with identical shape, indicating that the alkyl chains have a negligible influence on the electronic structures of the polymers. Figure 2a displays the UV−vis−near-IR (NIR) absorption spectra of the polymers in CB, which are composed of two primary absorption bands in the ranges of 300−500 and 500−900 nm, respectively. The

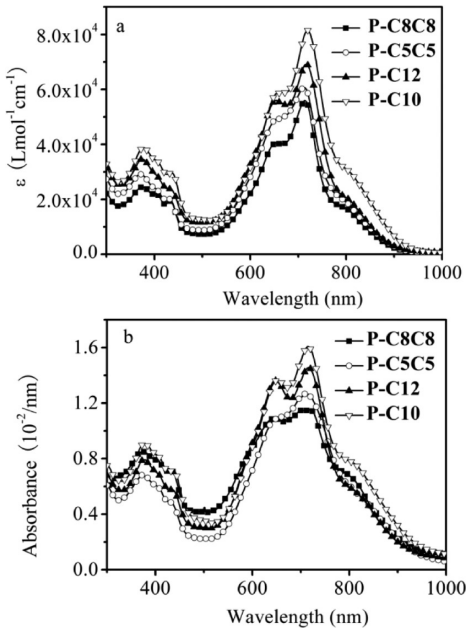

Figure 2. Solution (a; in CB with a concentration of 10^{-5} mol/L of repeating units) and film (b) UV−vis−NIR absorption spectra of the polymers. Films (~45 nm) were prepared by spin-casting the *o*-DCB solutions with a concentration of 6 mg/mL on quartz substrates.

strong absorption band at 500−900 nm is attributed to intramolecular charge transfer between the D and A units, and the other absorption band can be ascribed to a $\pi-\pi^*$ transition. The absorption maxima (λ_{max}) of **P-C8C8**, **P-C5C5**, **P-C12**, and **P-C10** are 712, 712, 719, and 718 nm, respectively. From solution to film, the absorption bands become broader, but no obvious shift in the absorption maxima was observed for all polymers. It is known that, in addition to the bandwidth of the absorption, a high absorption coefficient of the conjugated polymer is very important to efficiently harvest photons and thereby get a large short-circuit current in PSCs. As shown in Figure 2, both solution and film absorption coefficients of the polymers increase as the bulkiness of the alkyl chains decreases. This is consistent with an increase in the ratio of the conjugated backbone. **P-C10** exhibits the largest absorption capability. For example, in the film state, it absorbs 12% more light than **P-C8C8** in the range of 300−1000 nm at the same thickness. It is unusual that the polymers carrying straight alkyl substituents have stronger absorption than those containing branched alkyls. The alkyl chain in **P-C5C5** has one carbon less than that in **P-C12**. However, the absorption bands of **P-C12** are stronger than those of **P-C5C5**. The optical band gap (E_g^{opt}) values of these polymers, which are very similar and in the range of 1.31−1.35 eV, were calculated from the onset of the film absorption spectra and are listed in Table 2.

Film cyclic voltammetry (CV) measurements were performed in order to evaluate the electrochemical properties and estimate the energy levels of the polymers. CV curves are shown in Figure 3, and the data are outlined in Table 2. All polymers show reversible or quasi-reversible redox processes in both positive and negative potential regions. The HOMO and lowest unoccupied molecular orbital (LUMO) energy levels were estimated according to the equations HOMO = $-(4.80 + E_{onset}^{ox})$ eV and LUMO = $-(4.80 + E_{onset}^{re})$ eV, in which E_{onset}^{ox} and E_{onset}^{re} are the oxidation and reduction onset potentials, respectively. All polymers exhibited two reduction processes

dx.doi.org/10.1021/am401175v | ACS Appl. Mater. Interfaces 2013, 5, 5741−5747

Table 2. Optical and Electrochemical Properties of the Polymers

polymer	λ_{max} (nm) solution[a]	λ_{max} (nm) film	E_g^{opt} (eV)[b]	E_{onset}^{ox}(V)/HOMO (eV)[c]	E_{onset}^{re}(V)/LUMO (eV)[c]	E_g^{cv} (eV)[d]
P-C8C8	374, 653, 712	374, 646, 712	1.34	0.33/−5.13	−1.39/−3.41	1.72
P-C5C5	372, 652, 712	375, 648, 712	1.32	0.29/−5.09	−1.40/−3.40	1.69
P-C12	372, 648, 719	376, 647, 718	1.35	0.32/−5.12	−1.39/−3.41	1.71
P-C10	376, 655, 718	379, 652, 718	1.31	0.30/−5.10	−1.39/−3.41	1.69

[a]Measured in CB (concentration: 10^{-5} mol/L of the repeating unit). [b]E_g^{opt} was calculated from the film absorption onset. [c]HOMO and LUMO energy levels were calculated according to HOMO = −(4.80 + E_{onset}^{ox}) eV and LUMO = −(4.80 + E_{onset}^{ox}) eV, in which E_{onset}^{ox} and E_{onset}^{ox} are the oxidation and reduction onset potentials, respectively. [d]E_g^{cv} = −(LUMO − HOMO) eV.

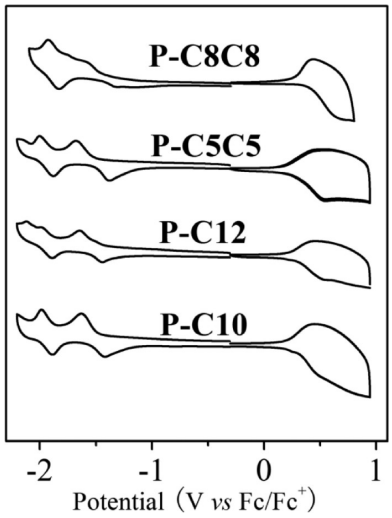

Figure 3. Thin-film CV curves of the polymers. The measurements were conducted in acetonitrile at a scan rate of 100 mV/s with Bu_4NPF_6 (0.1 mol/L) as the electrolyte. The films (~45 nm) on the working electrode were prepared by spin-casting from *o*-DCB solutions.

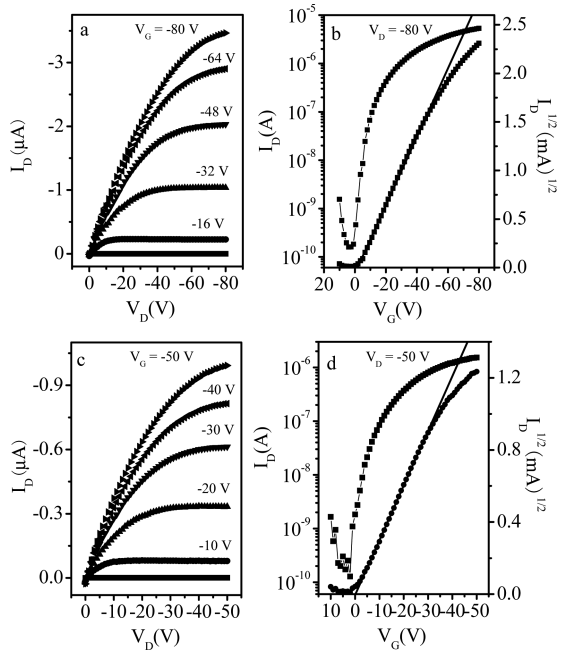

Figure 4. Typical output (a and c) and transfer (b and d) characteristics of OTFT devices of **P-C10** (a and b) and **P-C12** (c and d). The films were annealed at 150 °C for 20 min.

and one broad oxidation process. While the E_{onset}^{re} values of the polymers are identical (~−1.39 V), their E_{onset}^{ox} values have minor differences, which are 0.33, 0.29, 0.30, and 0.32 V for **P-C8C8**, **P-C5C5**, **P-C10**, and **P-C12**, respectively. The HOMO levels were determined to be −5.09 to −5.13 eV, and the LUMO levels were calculated to be about −3.41 eV for the polymers. The electrochemical band gaps are approximately 1.72 eV, which are 0.4−0.5 eV larger than the optical band gaps. The same phenomenon was also observed in other polymers.[40] These results indicate that the side chain has a negligible effect on the energy levels but has a strong impact on the absorption capability of the polymers.

Charge-Transporting Properties. In order to investigate the hole-transporting properties of **P-C8C8**, **P-C5C5**, **P-C12**, and **P−C10**, bottom-gate and top-contact OTFTs were fabricated, and the typical output and transfer plots are shown in Figure 4. All polymers show p-type characteristics, and the related data are listed in Table 3. The hole mobilities were deduced from the transfer characteristics of the device in a saturation regime. In a pristine film, the mobilities of **P-C8C8**, **P-C5C5**, **P-C12**, and **P-C10** were 6.0×10^{-4}, 6.5×10^{-4}, 3.5×10^{-3}, and 5.3×10^{-3} $cm^2/V{\cdot}s$, respectively. After thermal annealing at 150 °C, the mobilities were improved to 1.1×10^{-3}, 2.8×10^{-3}, 6.7×10^{-3}, and 1.1×10^{-2} $cm^2/V{\cdot}s$ for **P-C8C8**, **P-C5C5**, **P-C12**, and **P-C10**, respectively. The hole mobilities of the polymers were also measured with the space-charge-limited-current method with a device geometry of ITO/PEDOT:PSS (40 nm)/polymer (80 nm)/MoO_3 (6 nm)/Al (80 nm) and were 7.3×10^{-5}, 1.1×10^{-4}, 1.7×10^{-3}, and 3.4×10^{-3} $cm^2/V{\cdot}s$ for **P-C8C8**, **P-C5C5**, **P-C12**, and **P-C10**, respectively (Figure S3 in the Supporting Information). Obviously, the alkyl chain on the DTC unit has a strong impact on the hole mobility of the polymers. Although the polymer films are amorphous, we think that the bulkiness of the alkyl substituents still has an influence on the interchain packing of the polymers. The bulky alkyl substituents prevent the polymer backbones from close packing, inducing a weaker intermolecular interaction and therefore lower mobility.

Table 3. OTFT Device Performance of the Polymers

polymer	μ_{max}($cm^2/V{\cdot}s$)[a]	V_T (V)[b]	I_{on}/I_{off}[c]
P-C8C8	1.1×10^{-3}	−7.6	4.0×10^3
P-C5C5	2.8×10^{-3}	−6.4	1.5×10^4
P-C12	6.7×10^{-3}	−1.9	1.3×10^4
P-C10	1.1×10^{-2}	−0.23	2.1×10^4

[a]Mobility calculated from the saturation region after annealing at 150 °C for 20 min. [b]Threshold voltage. [c]Current on/off ratio.

Photovoltaic Properties. PSCs based on **P-C8C8**, **P-C5C5**, **P-C12**, and **P-C10** were fabricated with $PC_{71}BM$ as the acceptor material. The blend films of polymers and $PC_{71}BM$

dx.doi.org/10.1021/am401175v | ACS Appl. Mater. Interfaces 2013, 5, 5741−5747

with a thickness of ~90 nm were spin-cast from *o*-DCB solutions. It was found that the best weight ratio of polymer:$PC_{71}BM$ was 1:3 (w/w). Figure 5a displays the

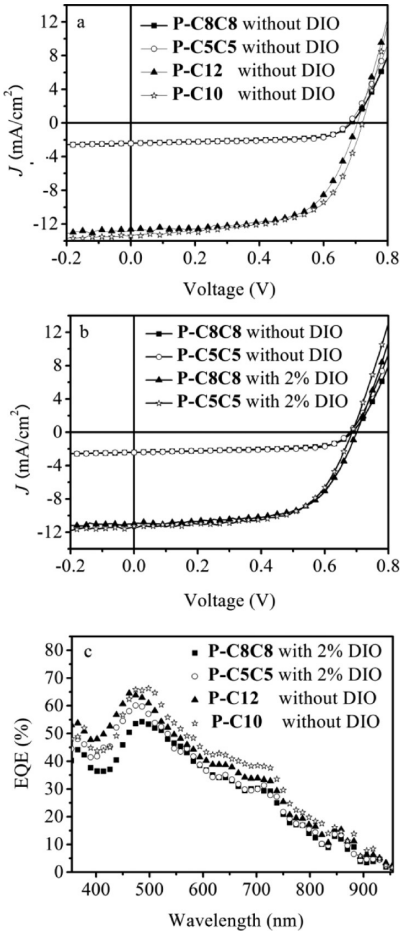

Figure 5. *J*–*V* characteristics of polymer:$PC_{71}BM$ [1:3 (w/w)] solar cells without the addition of DIO (a) and the solar cells based on **P-C8C8**:$PC_{71}BM$ [1:3 (w/w)] and **P-C5C5**:$PC_{71}BM$ [1:3 (w/w)] with and without the addition of DIO (b) under AM 1.5G illumination at 100 mW/cm^2 and EQE profiles of the solar cells with the addition of DIO for **P-C8C8** and **P-C5C5** and without the addition of DIO for **P-C10** and **P-C12** (c).

current–voltage (*J*–*V*) curves of the devices, and the data are summarized in Table 4. The V_{oc} and fill factor (FF) values of all of the devices were comparable in the range of 0.68–0.72 V and 61–65%, respectively. However, the J_{sc} values were quite

Table 4. Device Performance of the PSCs under AM 1.5G Illumination at 100 mW/cm^2[a]

polymer	solvent	V_{oc} (V)	J_{sc} (mA/cm^2)[b]	FF (%)	PCE (%)[b]
P-C8C8	*o*-DCB	0.69	2.32	61	0.97
	o-DCB + DIO	0.69	10.5 (10.1)	62	4.5 (4.3)
P-C5C5	*o*-DCB	0.68	2.51	65	1.1
	o-DCB + DIO	0.70	11.0 (10.3)	64	4.9 (4.6)
P-C12	*o*-DCB	0.70	12.1 (11.8)	64	5.4 (5.3)
P-C10	*o*-DCB	0.72	13.4 (12.9)	62	5.9 (5.7)

[a]Polymer:$PC_{71}BM$ = 1:3 (w/w); the thickness of the blend films is ~90 nm. [b]The values in parentheses are J_{sc} or PCE estimated from EQE profiles.

different. J_{sc} was 13.4 mA/cm^2 for **P-C10** and 12.1 mA/cm^2 for **P-C12**. In contrast, it was 2.32 mA/cm^2 for **P-C8C8** and 2.51 mA/cm^2 for **P-C5C5**. As a result, PCEs of **P-C10** and **P-C12** were 5.9 and 5.4%, respectively, which are 5–6 times those of **P-C8C8** and **P-C5C5** (0.97% and 1.1% for **P-C8C8** and **P-C5C5**, respectively).

Although the mobilities and absorption coefficients of **P-C8C8** and **P-C5C5** are lower than those of **P-C12** and **P-C10**, there should be other reasons responsible for much lower J_{sc} values of the devices based on **P-C8C8** and **P-C5C5**. To explore the reasons for this large variation in the device performance, transmission electron microscopy (TEM) images of the blend films were recorded and displayed in Figure 6. The

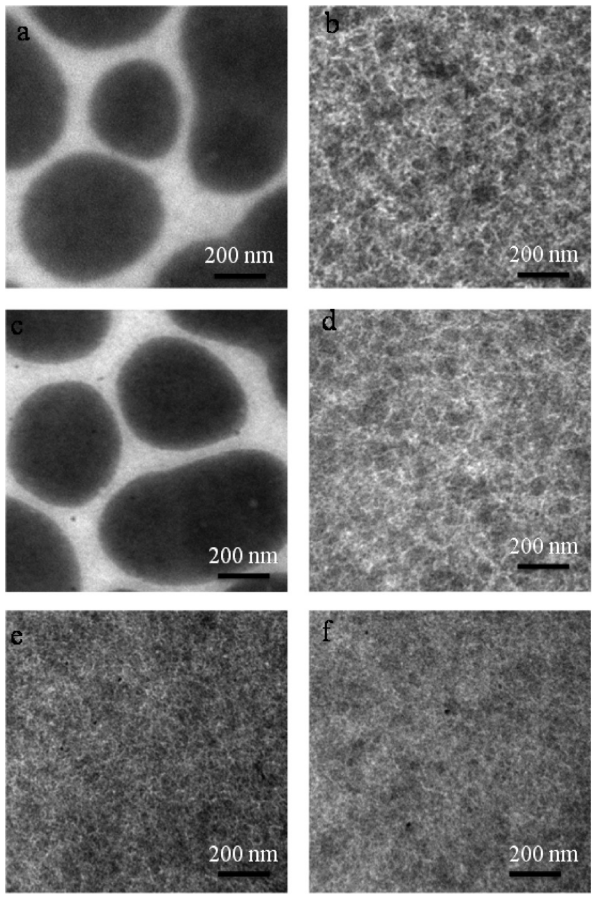

Figure 6. TEM images of the polymer:$PC_{71}BM$ [1:3 (w/w)] blend films: (a) **P-C8C8**, spin-cast from *o*-DCB; (b) **P-C8C8**, spin-cast from *o*-DCB containing 2 vol % DIO; (c) **P-C5C5**, spin-cast from *o*-DCB; (d) **P-C5C5**, spin-cast from *o*-DCB containing 2 vol % DIO; (e) **P-C10**, spin-cast from *o*-DCB; (f) **P-C12**, spin-cast from *o*-DCB.

films of **P-C8C8** and **P-C5C5** clearly show large domains of aggregated $PC_{71}BM$. In contrast, the films of **P-C12** and **P-C10** display fine features of phase separation with domain sizes of <15 nm. Although the effect of the alkyl chain on the blend film morphology was also observed by us and others before,[28,45] such a dramatic film morphology change caused by structural alternation of the alkyl substituent (linear vs branched) is unusual. This phenomenon may be attributed to the different solubilities of the polymers.[47] The polymers carrying branched alkyl chains, i.e., **P-C8C8** and **P-C5C5**, have higher solubility in the processing solvent *o*-DCB than $PC_{71}BM$. As a result, $PC_{71}BM$ molecules precipitated out first in the film formation

dx.doi.org/10.1021/am401175v | ACS Appl. Mater. Interfaces 2013, 5, 5741–5747

process to form large domains. In contrast, **P-C12** and **P-C10** have relatively lower solubility and should solidify in a short time in the spin-casting process, leaving less space and time for $PC_{71}BM$ molecules to form large domains. This observation implies that both the structures of the polymer backbone and the alkyl side chains have to be finely optimized for conjugated polymers used for BHJ PSCs. Strong phase separation and large domain size can diminish exciton migration to the donor/acceptor interface for charge separation, resulting in low J_{sc} values. It is known that the morphology of the active layer of PSCs can be optimized via the rational choice of the processing additives.[48−50] As shown in Figure 6b,d, upon addition of 2.0 vol % 1,8-diiodooctane (DIO) into *o*-DCB as the additive, the film morphology of **P-C8C8** and **P-C5C5** was improved greatly. Consequently, the J_{sc} values of the devices based on **P-C8C8** and **P-C5C5** were improved to 10.5 and 11.0 mA/cm^2, respectively. Consequently, the PCEs were enhanced to 4.5% for **P-C8C8** and 4.9% for **P-C5C5**. No further improvement of the device performance for **P-C10** and **P-C12** was observed when DIO was added. Nevertheless, the PCE of the devices based on **P-C10** is among the best for DPP-based D−A conjugated polymers.[35,51−55] The representative external quantum efficiency (EQE) profiles of the PSCs are displayed in Figure 5b. The devices based on all four polymers exhibited photoresponse in a very broad range from 300 to 900 nm, consistent with the low-band-gap nature of the polymers. To verify the accuracy of device performance measurements, J_{sc} values of the typical devices were also estimated from EQE profiles under AM 1.5 illumination condition (100 mW/cm^2). The resulting J_{sc} and PCE values are also listed in Table 4, which are largely consistent with the measured values.

4. CONCLUSIONS

A series of D−A conjugated polymers, i.e., **P-C8C8**, **P-C5C5**, **P-C12**, and **P-C10**, which contain a five-ring heteroacene (dithieno[2,3-*b*:7,6-*b*]carbazole, DTC) and DPP as D and A units, were synthesized, and the effect of the alkyl substituents on the optoelectronic properties of the polymers was investigated. The alkyl side chain on the nitrogen atom in the DTC unit has little effect on the energy levels and the absorption maxima wavelengths but has a noticeable influence on the absorption capability, charge-transporting ability, and miscibility with $PC_{71}BM$. The polymers carrying straight alkyl chains on the DTC unit exhibit stronger absorption, higher mobility, and much better miscibility with $PC_{71}BM$ and, consequently, show much higher solar cell performance. **P-C10** exhibits the best PSC performance. A V_{oc} of 0.72, a J_{sc} of 13.4 mA/cm^2, and a FF of 62% were achieved, leading to a PCE of 5.9%.

■ ASSOCIATED CONTENT

Supporting Information

Synthesis of monomers and polymers, DSC profiles of the polymers, output and transfer characteristics of OTFT devices of **P-C8C8** and **P-C5C5**, hole-only device performance of the polymers, and AFM images of polymer/$PC_{71}BM$ films. This material is available free of charge via the Internet at http://pubs.acs.org.

■ AUTHOR INFORMATION

Corresponding Author

*E-mail: yhgeng@ciac.jl.cn.

Notes

The authors declare no competing financial interest.

■ ACKNOWLEDGMENTS

This work is supported by the National Basic Research Program of China (973 Project, Grant 2009CB623603) of Chinese Ministry of Science and Technology and the National Science Foundation of China (Grants 50833004 and 51211120187).

■ REFERENCES

(1) Nielsen, T. D.; Cruickshank, C.; Foged, S.; Thorsen, J.; Krebs, F. C. *Sol. Energy Mater. Sol. Cells* **2010**, *94*, 1553−1571.
(2) Krebs, F. C. *Sol. Energy Mater. Sol. Cells* **2009**, *93*, 394−412.
(3) Li, G.; Zhu, R.; Yang, Y. *Nat. Photonics* **2012**, *6*, 153−161.
(4) He, Z. C.; Zhong, C. M.; Su, S. J.; Xu, M.; Wu, H. B.; Cao, Y. *Nat. Photonics* **2012**, *6*, 591−595.
(5) Small, C. E.; Chen, S.; Subbiah, J.; Amb, C. M.; Tsang, S.-W.; Lai, T.-H.; Reynolds, J. R.; So, F. *Nat. Photonics* **2012**, *6*, 115−120.
(6) Li, X. H.; Choy, W. C. H.; Huo, L. J.; Xie, F. X.; Sha, W. E. I.; Ding, B. F.; Guo, X.; Li, Y. F.; Hou, J. H.; You, J. B.; Yang, Y. *Adv. Mater.* **2012**, *24*, 3046−3052.
(7) He, Z. C.; Zhong, C. M.; Huang, X.; Wong, W.-Y.; Wu, H. B.; Chen, L. W.; Su, S. J.; Cao, Y. *Adv. Mater.* **2011**, *23*, 4636−4643.
(8) Yang, T. B.; Wang, M.; Duan, C. H.; Hu, X. W.; Huang, L.; Peng, J. B.; Huang, F.; Gong, X. *Energy Environ. Sci.* **2012**, *5*, 8208−8214.
(9) Son, H. J.; Wang, W.; Xu, T.; Liang, Y. Y.; Wu, Y.; Li, G.; Yu, L. P. *J. Am. Chem. Soc.* **2011**, *133*, 1885−1894.
(10) Amb, C. M.; Chen, S.; Graham, K. R.; Subbiah, J.; Small, C. E.; So, F.; Reynolds, J. R. *J. Am. Chem. Soc.* **2011**, *133*, 10062−10065.
(11) Price, S. C.; Stuart, A. C.; Yang, L. Q.; Zhou, H. X.; You, W. *J. Am. Chem. Soc.* **2011**, *133*, 4625−4631.
(12) Chu, T.-Y.; Lu, J. P.; Beaupré, S.; Zhang, Y. G.; Pouliot, J.-R.; Wakim, S.; Zhou, J. Y.; Leclerc, M.; Li, Z.; Ding, J. F.; Tao, Y. *J. Am. Chem. Soc.* **2011**, *133*, 4250−4253.
(13) Huang, Y.; Guo, X.; Liu, F.; Huo, L. J.; Chen, Y. N.; Russell, T. P.; Han, C. C.; Li, Y. F.; Hou, J. H. *Adv. Mater.* **2012**, *24*, 3383−3389.
(14) Huo, L. J.; Zhang, S. Q.; Guo, X.; Xu, F.; Li, Y. F.; Hou, J. H. *Angew. Chem., Int. Ed.* **2011**, *50*, 9697−9702.
(15) Zhou, H. X.; Yang, L. Q.; Stuart, A. C.; Price, S. C.; Liu, S. B.; You, W. *Angew. Chem., Int. Ed.* **2011**, *50*, 2995−2998.
(16) Liang, Y. Y.; Xu, Z.; Xia, J. B.; Tsai, S.-T.; Wu, Y.; Li, G.; Ray, C.; Yu, L. P. *Adv. Mater.* **2010**, *22*, E135−E138.
(17) Boudreault, P. L. T.; Najari, A.; Leclerc, M. *Chem. Mater.* **2011**, *23*, 456−469.
(18) Beaujuge, P. M.; Frechet, J. M. J. *J. Am. Chem. Soc.* **2011**, *133*, 20009−20029.
(19) Li, Y. F. *Acc. Chem. Res.* **2012**, *45*, 723−733.
(20) Blouin, N.; Michaud, A.; Leclerc, M. *Adv. Mater.* **2007**, *19*, 2295−2300.
(21) Park, S. H.; Roy, A.; Beaupré, S.; Cho, S.; Coates, N.; Moon, J. S.; Moses, D.; Leclerc, M.; Lee, K.; Heeger, A. J. *Nat. Photonics* **2009**, *3*, 297−302.
(22) Lu, J. P.; Liang, F. S.; Drolet, N.; Ding, J. F.; Tao, Y.; Movileanua, R. *Chem. Commun.* **2008**, 5315−5317.
(23) Zhu, Z. G.; Waller, D.; Gaudiana, R.; Morana, M.; Mühlbacher, D.; Scharber, M.; Brabec, C. *Macromolecules* **2007**, *40*, 1981−1986.
(24) Mühlbacher, D.; Scharber, M.; Morana, M.; Zhu, Z. G.; Waller, D.; Gaudiana, R.; Brabec, C. *Adv. Mater.* **2006**, *18*, 2884−2889.
(25) Hou, J. H.; Chen, H.-Y.; Zhang, S. Q.; Li, G.; Yang, Y. *J. Am. Chem. Soc.* **2008**, *130*, 16144−16145.
(26) Zheng, Q. D.; Jung, B. J.; Sun, J.; Katz, H. E. *J. Am. Chem. Soc.* **2010**, *132*, 5394−5404.
(27) Cheng, Y.-J.; Wu, J.-S.; Shih, P.-I.; Chang, C.-Y.; Jwo, P.-C.; Kao, W.-S.; Hsu, C.-S. *Chem. Mater.* **2010**, *23*, 2361−2369.
(28) Bronstein, H.; Leem, D. S.; Hamilton, R.; Woebkenberg, P.; King, S.; Zhang, W. M.; R. Ashraf, S.; Heeney, , M.; Anthopoulos, , T.

D.; de Mello, , J.; McCulloch, , I. *Macromolecules* **2011**, *44*, 6649−6652.
(29) Cheng, Y.-J.; Chen, C.-H.; Lin, Y.-S.; Chang, C.-Y.; Hsu, C.-S. *Chem. Mater.* **2011**, *23*, 5086−5075.
(30) Schroeder, B. C.; Huang, Z. G.; Ashraf, R. S.; Smith, J.; Angelo, P.; Watkins, S. E.; Anthopoulos, T. D.; Durrant, J. R.; McCulloch, I. *Adv. Funct. Mater.* **2012**, *22*, 1663−1670.
(31) Wu, J.-S.; Cheng, Y.-J.; Lin, T.-Y.; Chang, C.-Y.; Shih, P.-I.; Hsu, C.-S. *Adv. Funct. Mater.* **2012**, *22*, 1711−1722.
(32) Zhang, Y.; Zou, J. Y.; Yip, H.-L.; Chen, K.-S.; Zeigler, D. F.; Sun, Y.; Jen, A. K.-Y. *Chem. Mater.* **2011**, *23*, 2289−2291.
(33) Xu, Y.-X.; Chueh, C.-C.; Yip, H.-L.; Ding, F. Z.; Li, Y.-X.; Li, C. Z.; Li, X. S.; Chen, W.-C.; Jen, A.K.-Y. *Adv. Mater.* **2012**, *24*, 6356−6361.
(34) Zhang, F. L.; Jespersen, K. G.; Björström, C.; Svensson, M.; Andersson, M. R.; Sundström, V.; Magnusson, K.; Moons, E.; Yartsev, A.; Inganäs, O. *Adv. Funct. Mater.* **2006**, *16*, 667−674.
(35) Wienk, M. M.; Turbiez, M.; Gilot, J.; Janssen, R. A. J. *Adv. Mater.* **2008**, *20*, 2556−2560.
(36) Zou, Y. P.; Najari, A.; Berrouard, P.; Beaupré, S.; Aïch, B. R.; Tao, Y.; Leclerc, M. *J. Am. Chem. Soc.* **2010**, *132*, 5330−5331.
(37) Liu, J.; Shao, S. Y.; Fang, G.; Meng, B.; Xie, Z. Y.; Wang, L. X. *Adv. Mater.* **2012**, *24*, 2774−2779.
(38) Liu, J.; Shao, S. Y.; Fang, G.; Meng, B.; Xie, Z. Y.; Wang, L. X. *Appl. Phys. Lett.* **2012**, *100*, 213906.
(39) Chen, Y. G.; Tian, H. K.; Yan, D. H.; Geng, Y. H.; Wang, F. S. *Macromolecules* **2011**, *44*, 5178−5185.
(40) Deng, Y. F.; Chen, Y. G.; Zhang, X. J.; Tian, H. K.; Bao, C.; Yan, D. H.; Geng, Y. H.; Wang, F. S. *Macromolecules* **2012**, *45*, 8621−8627.
(41) Li, Z.; Zhang, Y. G.; Tsang, S.-W.; Du, X. M.; Zhou, J. Y.; Tao, Y.; Ding, J. F. *J. Phys. Chem. C* **2011**, *115*, 18002−18009.
(42) Biniek, L.; Fall, S.; Chochos, C. L.; Anokhin, D. V.; Ivanov, D. A.; Leclerc, N.; Lévêque, P.; Heiser, T. *Macromolecules* **2010**, *43*, 9779−9786.
(43) Piliego, C.; Holcombe, T. W.; Douglas, J. D.; Woo, C. H.; Beaujuge, P. M.; Fréchet, J. M. J. *J. Am. Chem. Soc.* **2010**, *132*, 7595−7597.
(44) Szarko, J. M.; Guo, J. C.; Liang, Y. Y.; Lee, B.; Rolczynski, B. S.; Strzalka, J.; Xu, T.; Loser, S.; Marks, T. J.; Yu, L. P.; Chen, L. X. *Adv. Mater.* **2010**, *22*, 5468−5472.
(45) Yue, W.; Zhao, Y.; Shao, S. Y.; Tian, H. K.; Xie, Z. Y.; Geng, Y. H.; Wang, F. S. *J. Mater. Chem.* **2009**, *19*, 2199−2260.
(46) Shao, S. Y.; Liu, J.; Zhang, J. D.; Zhang, B. H.; Xie, Z. Y.; Geng, Y. H.; Wang, L. X. *ACS Appl. Mater. Interfaces* **2012**, *4*, 5704−5710.
(47) Chu, T.-Y.; Lu, J. P.; Beaupré, S.; Zhang, Y. G.; Pouliot, J.-R.; Zhou, J. Y.; Najari, A.; Leclerc, M.; Tao, Y. *Adv. Funct. Mater.* **2012**, *22*, 2345−2351.
(48) Peet, J.; Kim, J. Y.; Coates, N. E.; Ma, W. L.; Moses, D.; Heeger, A. J.; Bazan, G. C. *Nat. Mater.* **2007**, *6*, 497−500.
(49) Coates, N. E.; Hwang, I.-W.; Peet, J.; Bazan, G. C.; Moses, D.; Heeger, A. J. *Appl. Phys. Lett.* **2008**, *93*, 072105.
(50) Lee, J. K.; Ma, W. L.; Brabec, C. J.; Yuen, J.; Moon, J. S.; Kim, J. Y.; Lee, K.; Bazan, G. C.; Heeger, A. J. *J. Am. Chem. Soc.* **2008**, *130*, 3619−3623.
(51) Bronstein, H.; Chen, Z. Y.; Ashraf, R. S.; Zhang, W. M.; Du, J. P.; Durrant, J. R.; Tuladhar, P. S.; Song, K.; Watkins, S. E.; Geerts, Y.; Wienk, M. M.; Janssen, R. A. J.; Anthopoulos, T.; Sirringhaus, H.; Heeney, M.; McCulloch, I. *J. Am. Chem. Soc.* **2011**, *133*, 3272−3275.
(52) Bijleveld, J. C.; Gevaerts, V. S.; Nuzzo, D. D.; Turbiez, M.; Mathijssen, S. G. J.; de Leeuw, D. M.; Wienk, M. M.; Janssen, R. A. J. *Adv. Mater.* **2010**, *22*, E242−E246.
(53) Bijleveld, J. C.; Zoombelt, A. P.; Mathijssen, S. G. J.; Wienk, M. M.; Turbiez, M.; de Leeuw, D. M.; Janssen, R. A. J. *J. Am. Chem. Soc.* **2009**, *131*, 16616−16617.
(54) Dou, L. T.; Gao, J.; Richard, E.; You, J. B.; Chen, C.-C.; Cha, K. C.; He, Y. J.; Li, G.; Yang, Y. *J. Am. Chem. Soc.* **2012**, *134*, 10071−10079.
(55) Li, W. W.; Roelofs, W. S. C.; Wienk, M. M.; Janssen, R. A. J. *J. Am. Chem. Soc.* **2012**, *134*, 13787−13795.